

Two-Dimensional Simulations of the Thermonuclear Runaway in an Accreted Atmosphere of a C+O White Dwarf

A. Kercek¹, W. Hillebrandt¹, and J. W. Truran²

¹ Max Planck Institut für Astrophysik, Karl-Schwarzschild-Strasse 1, D-85740 Garching, Germany

² Department of Astronomy and Astrophysics, Enrico Fermi Institute, University of Chicago, Chicago, IL 60637, USA

Abstract. We present the results of two-dimensional calculations of turbulent nuclear burning of hydrogen-rich material accreted onto a white dwarf of $1.0 M_{\odot}$. The main aim of the present paper is to investigate the question as to whether and how the general properties of the burning are affected by numerical resolution effects. In particular, we want to see whether or not convective overshooting into the surface layers of the C+O white dwarf can lead to self-enrichment of the initially solar composition of the hydrogen-rich envelope with carbon and oxygen from the underlying white dwarf core.

Our explicit hydrodynamic code is based on the PPM-method and computes the onset of the thermonuclear runaway on a Cartesian grid. Only part of the white dwarf's surface is covered by the computational grid and curvature effects are ignored. In contrast to previous works we do not observe fast mixing of carbon and oxygen from the white dwarf's surface into the envelope by violent overshooting of large eddies. The main features of the flow fields in our simulations are the appearance of small persistent coherent structures of very high vorticity (and velocity) compared to the background flow. Their typical linear scales are about 10 to 20 grid zones and thus their physical size depends on the numerical resolution, i.e., their size decreases with increasing resolution. For the early phase of the thermonuclear runaway (TNR) they dominate the flow patterns and result in very little overshoot and mixing. Only at late times, after steady slow mixing and with increasing nuclear energy production, do these structures become weak, but show up again once hydrogen has mainly been burnt and the energy generation rate drops.

On the other hand, there are no big differences between high and low resolution simulations, as far as the overall properties of the TNR are concerned. The two simulations which are presented here show only moderate differences in spatially integrated quantities such as laterally averaged temperature, energy generation rate, and chemical composition. We have not expanded both simulations equally long, but for the physical time under consideration the

major difference seems to be that the highly resolved simulation is a bit less violent. In conclusion, we do find some self-enrichment, but on time-scales much longer than in previous calculations.

Key words: Stars : novae, cataclysmic variables - white dwarfs; Physical data and processes : convection - hydrodynamics - nuclear reactions, nucleosynthesis, abundances

1. Introduction

It is generally accepted that the outburst of a classical nova is caused by a thermonuclear runaway (TNR) in the accreted hydrogen-rich envelope on top of a white dwarf in a close binary system (Starrfield 1989; Starrfield 1983; Starrfield 1995; Truran 1982; Truran 1990). Detailed one-dimensional spherically symmetric models of the runaway, based on realistic nuclear reaction rate networks but using the mixing-length theory (MLT) of convection, have been studied extensively (Starrfield, Sparks & Truran 1974, 1985; Prialnik, Shara & Shaviv 1978; Mac Donald 1980), and the results are in good agreement with observational data, such as the total amount of energy released and the metallicity and the abundances of the expelled envelope material.

However, using the MLT to model the runaway is very questionable, as can be seen from simple arguments. In general terms, the physics of the TNR can be described as follows. For a white dwarf accreting matter from a companion star of roughly solar composition, during the accretion process the temperature at the base of the envelope and the nuclear energy release increase steadily but slowly. Once the temperature exceeds about $2 \cdot 10^7$ K heat conduction can no longer transport the energy released by nuclear reactions fast enough and the envelope becomes unstable to convection. However, because of electron degeneracy the nuclear energy released does not go into lifting off the envelope at this stage, but the temperature

increases further and the TNR proceeds until the electron degeneracy is removed and an overall expansion sets in. At the onset of the violent burning phase the temperature at the bottom of the envelope is about 10^8 K and it lasts for several minutes. Energy production is dominated by the β -limited CNO-cycle since the temperatures never exceed $4 \cdot 10^8$ K (see, e.g., Wallace & Woosley (1981)). Therefore, the energy production per unit mass is independent of temperature and density and is just a linear function of metallicity (Wallace & Woosley 1981). The limitation of the nuclear energy generation rate is the reason why hydrogen burning on top of a white dwarf is different from, say, the carbon-burning deflagration wave inside a Chandrasekhar-mass white dwarf. In the latter case, due to the temperature sensitivity of the energy generation rate and the small thermal width of the burning region a flame forms and is passively advected by the turbulent motions. Combustion is said to be in the “flamelet” regime. In contrast, in the phase of CNO-limited hydrogen burning on top of a white dwarf burning is always slow compared to convective turn-over and combustion takes place in the so-called “well-stirred” regime for which either direct numerical simulations have to be carried out or pdf-methods have to be applied. In either case, the treatment of convection is crucial and requires special care because convection dominates over burning.

A second aspect which makes reliable numerical simulations of novae very difficult is the fact that due to diffusion and coupling to hydrodynamic flows (especially convective overshooting (Woosley 1986)) there can be a significant increase of the energy production rate by mixing C and O from the white dwarf core into the envelope. The β -limited CNO-cycle operates no longer in a strict equilibrium, but due to the increase of the C and O abundances in mixed zones the energy generation rate is time-dependent and couples to the mixing processes in a very non-linear manner: Violent motions can cause mixing which in turn may make the motions even more violent. It was this effect that lead to fast self-enrichment and a rapid temperature rise in the two-dimensional direct simulations of Glasner, Livne & Truran (1997).

A third question concerns the ignition process. One dimensional models with spherical symmetry consider a global and simultaneous ignition at the bottom layer of the envelope (global TNR or GTNR). However, according to Shara (1981,1982) also a local TNR (LTNR) is possible, because of temperature inhomogeneities arising from magnetic fields, rotation and non-spherically symmetric accretion. Since it would take years to spread the combustion front from a LTNR over the white dwarf’s surface diffusively by radiative transport and thermal conduction (Shara 1981,1982), Fryxell & Woosley (1982) discuss that heat transport by mass motions as a multidimensional effect dominates over diffusion. For typical situations at peak temperature they find laminar burning velocities of about $v_{\text{lam}} = 30$ cm/s only. In contrast, estimating the ef-

fective burning velocity caused by small-scale turbulence motions to be

$$v_{\text{burn}} = v_{\text{lam}} + \left(\frac{h_p v_c}{\tau_{\text{burn}}} \right), \quad (1)$$

where h_p is the pressure scale height, and v_c the typical convective velocity, they obtain $v_{\text{burn}} \sim 10$ km/s for a typical nova model. So again, multi-dimensional effects can be crucial for the TNR.

To date, not very many multi-dimensional studies exist which deal with the various questions raised above. Shankar, Arnett & Fryxell (1992); Shankar & Arnett (1994); Glasner & Livne (1995); Glasner, Livne, & Truran (1995) and Glasner, Livne, & Truran (1997) were the first to carry out two-dimensional direct simulations of TNRs. In the most recent computation (Glasner, Livne & Truran 1997) no initial enrichment of carbon and oxygen was necessary to initiate a rapid TNR which, likely, will lead to an outburst similar to that of a classical nova. In their case violent large eddies were responsible for considerable mixing of envelope and core matter. Their computations were performed with the (implicit) VULCAN-code (Livne 1993) in spherical coordinates for a slice of 0.1π radians with reflecting boundaries at the bottom and on both sides.

Because their results are so important and because sometimes numerical effects cannot be separated from physical ones easily we decided to perform independent simulations based upon a different hydro-code (PROMETHEUS; Fryxell, Müller & Arnett (1989)). Moreover, we decided to ignore curvature effects and to represent the surface layers of the white dwarf as well as its envelope by a plane-parallel sheet. The advantage of this approach is that we can use periodic boundary conditions and thereby avoid common problems of numerical simulations of free convection, namely that reflecting boundaries may act like a containment and may affect the flow patterns in an unphysical way. In spherical coordinates with the polar axis singled out one cannot use periodic boundary conditions. We will come back to this point later in Sec. 4 when we interpret our results and compare them with Glasner, Livne & Truran (1997).

In the following we present the first results of our two dimensional (2-d) simulations starting from the same initial conditions as Glasner, Livne & Truran (1997). We performed the simulations with two different Cartesian grids covering the same domain as in Glasner, Livne & Truran (1997). The first grid has approximately the same numerical resolution as was used by Glasner, Livne & Truran (1997), and the second one uses 5 times more zones in each direction. In Sec. 2 we give a description of our numerical method, including the hydro-code, the nuclear reaction network, and details of the initial conditions. In Sec. 3 we present the results, and Sec. 4 is devoted to a discussion and, in particular, to a comparison with the work of Glasner, Livne & Truran (1997). The fact that according to our work 2-d simulations predict that during

most of the TNR large scale motions do not dominate the evolution gives us hope that going to the full 3-d problem may not change all our conclusions. 3-d calculations which will proof or disproof this conjecture are under way and will be published in a subsequent paper.

2. The code and initial conditions

Our calculations were performed with a slightly modified version of PROMETHEUS, an Eulerian code based on a second order Godunov method with piecewise parabolic interpolation of the conserved quantities for solving the hydrodynamic equations, as worked out by Colella & Woodward (1984) and Fryxell, Müller & Arnett (1989). Since this code is used frequently by various groups (see, e.g., Müller (1994,1997) Shankar & Arnett (1994) and Niemeyer & Hillebrandt (1995)) we do not give a detailed description here or provide any numerical tests. We want to mention in passing, however, that we had to change a few things in the original version of the code to make it applicable to the problem under consideration. First, a challenging problem was to keep the initial model stable over several thousand dynamical time scales if nuclear reactions were suppressed. The second problem was the presence of huge gradients at the core-envelope interface which lead to unacceptable numerical diffusion.

In order to get a stable initial model we solved the equations of hydrostatic equilibrium for the pressure with a Runge-Kutta-solver, using the density and composition profiles of the initial model of Glasner, Livne & Truran (1997), which will be described in more detail later in this chapter, and our equation of state. Next we mapped this density distribution on to the grid required by PROMETHEUS. The deviations from the original model of Livne and Glasner were less than 1 % in pressure and density.

The huge gradients at the core-envelope interface required special attention since gravity in most versions of PROMETHEUS is included by calculating the gravitational acceleration *after* each hydro time step. Since PROMETHEUS is a conservative second order Godunov scheme one cannot impose hydrostatic equilibrium directly. Consequently, pressure gradients are not balanced exactly by gravity. The accuracy one can reach is about 0.1 % which causes a net acceleration for the core-envelope-interface resulting in a systematic slow but significant outward motion of the interface.

To overcome this problem we have treated the time evolution of the gravitational acceleration in a more symmetric way. It was included by calculating its action prior to and after the hydro timesteps with weighting factors f and $(1 - f)$, respectively. We found that for $f = 0.12$ the interface stayed in place for several thousand dynamical timescales, after the model had been relaxed, with nuclear reactions being turned off.

In fact, we found that these modifications of the original PROMETHEUS scheme were significant but not cru-

cial. As a test, we performed a 2-d simulation with nuclear reactions turned on for $f=0$ where the interface was moving outwards with the same speed as in the 1-d case without nuclear burning. We realized that except for the moving of the transition region and some unphysical strong heating at the inner reflecting boundary the flow fields did not change by much. The main difference was a slightly higher energy production rate for the $f=0$ case since numerical diffusion mixed additional core material into the burning region of the envelope.

Finally, the code was changed to run efficiently on massively parallel computers such as the CRAY T3E by means of explicit message passing.

In our version of PROMETHEUS nuclear reactions are incorporated by solving together with the hydrodynamics a nuclear reaction network including 12 nuclear species, i.e., ^1H , ^4He , ^{12}C , ^{13}C , ^{13}N , ^{14}N , ^{15}N , ^{14}O , ^{15}O , ^{16}O , ^{17}O , and ^{17}F , linked by reactions described in Wallace & Woosley (1981). The reaction rates are taken from Thielemann (1996). Following Müller (1986), we solve the network equations and the energy source equation simultaneously to avoid numerical instabilities.

For a given density ρ the network equations and the energy source equation have the following form:

$$\dot{Y}_i - F(Y_j, T) = 0 \quad (2)$$

$$\dot{\epsilon} - H(Y_j, T) = 0, \quad (3)$$

where Y_i are the nuclear abundances, $\dot{\epsilon}$ is the energy production rate per unit mass, $i,j = 1 \dots N$, and N is the number of nuclear species. F and H denote nonlinear functions of the arguments. This system of equations is solved implicitly from time t^n to $t^{n+1} = t^n + \delta t$ according to

$$Y_i^{n+1} - Y_i^n - \delta t \cdot F(Y_j^{n+1}, T^{n+1}) = 0 \quad (4)$$

$$\epsilon^{n+1} - \epsilon^n - \delta t \cdot H(Y_j^{n+1}, T^{n+1}) = 0 \quad (5)$$

by a Newton-Raphson-solver.

The coupling to the hydrodynamic equations is done by solving this system with Y_j^n , T^n and ρ^n after hydro time step n with step size δt is executed, and incorporating the results, namely Y_i^{n+1} and ϵ^{n+1} into the hydrodynamic equations in the next time step $n+1$. Heat conduction, magnetic fields, radiation and a possible rotation of the white dwarf are ignored.

Here, we use the same initial model for our two-dimensional calculations as Glasner, Livne, & Truran (1997). Since for the problem of simulating subsonic convection in an explicit scheme such as ours the time step (here: \sim milliseconds) is limited by the cell size and the local sound speed, it is not possible to calculate by means of such schemes the whole accretion process (several 10^5 years) until the TNR takes place. Moreover, even for an implicit code, such as VULCAN, solving the full problem in 2-d is nearly impossible. Therefore the accretion phase and the slow stages of the burning were calculated by Glasner, Livne & Truran (1997) using a one dimensional implicit hydro code (Glasner & Truran 1996).

During this early phase hydrogen-rich matter of solar composition ($Z = 0.02$) is accreted onto the surface of a $1 M_{\odot}$ C+O white dwarf at a accretion rate of $5.0 \cdot 10^{-9} M_{\odot} \text{yr}^{-1}$. As at the bottom of the envelope the temperature rises convection sets in. Convection is taken into account by the MLT in the one dimensional model. The model we obtained from A. Glasner and E. Livne provided the density, temperature, entropy, and composition profiles at the point at which the temperature at the bottom of the envelope had already reached 10^8 K. The mass of the hydrogen shell is about $2 \cdot 10^{-5} M_{\odot}$. We mapped this model onto a radial row of our 2-d grid and relaxed it for several hundred dynamical time scales and then mapped it onto the full 2-d grid. The calculations were done with two different resolutions of a domain nearly identical to what has been used by Glasner, Livne & Truran (1997). This means that the grid covers 100 km of the outer part of the white dwarf and 1000 km of the envelope, radially, and ~ 1800 km in the lateral direction, corresponding to the outer part of a 0.1π segment in spherical coordinates. But both grids are Cartesian and the curvature of the WD surface is ignored for reasons given earlier. The coarser computational grid consists of 100 uneven radial zones and 220 lateral zones which are equally spaced. Hence the spatial resolution within the white dwarf and the first layers of the envelope is about $5 \text{ km} \times 8 \text{ km}$ in this case. The finer computational grid consists of 500 uneven radial zones and 1000 lateral zones which are equally spaced. Here the spatial resolution within the white dwarf and the first few layers of the envelope is about $1 \text{ km} \times 2 \text{ km}$.

Our equation of state consists of the ideal Boltzmann gases of the nuclei under consideration, an electron gas component with arbitrary degeneracy and a photon gas component.

Finally, the boundary conditions and the initial perturbation have to be specified. Here we use a reflecting boundary at the bottom and an outflow boundary at the top of the grid. Periodic boundary conditions are applied laterally. The model is initially perturbed by increasing temperature in one zone of the bottom layer of the envelope by 1% in both cases. The further evolution is then followed for about 1400 physical seconds in the case of the low resolution grid and for about 180 physical seconds for the high resolution run. In the next Section we summarize the results of both calculations and compare them.

3. Results

3.1. The low resolution simulation

After the ignition of one zone the burning remains local for a few seconds (Fig. 1b). Once the temperature has gone up a bit a first local TNR sets in. The burning front propagates laterally with a velocity of about 15 km/s which is very close to the lateral spread by small scale turbulence as was estimated by Fryxell & Woosley (1982). This

means that it should take over 100 s to ignite the entire bottom layer of our computational domain by small scale turbulence. However, this argument ignores the capability of sound waves to ignite an isothermal layer which is close to the ignition temperature. In fact, we find that spreading happens essentially on a sound travel time once a sufficiently large volume burns and sound waves are emitted from this region, and a full horizontal layer of the computational grid burns after about 14 s (Fig. 1c). Of course, our initial conditions, namely an isothermal layer very close to ignition temperature, enhance this effect and, in reality, small scale turbulence may turn out to be more important. Already 20 s after ignition the information about the location of the ignition point is largely lost. During the following 500 s the mean energy generation rate in the most violently burning shells is slowly increasing from about 10^{13} erg/g/s to over 10^{15} erg/g/s (Fig. 2), and individual zones reach up to $\sim 3 \cdot 10^{15}$ erg/g/s (Fig. 10b).

In detail, the thermal history of the convectively burning shells turns out to be rather complicated. During the first 25 seconds cooling by convective mixing of cold envelope material into the burning region is slightly more efficient than nuclear energy release. Thus the maximum temperature drops a bit before rising rather moderately, and we do not find a change into a fierce runaway (Fig. 3a). This first result does not come as a surprise. In fact, it is consistent with 1-d models which do not assume initial enrichment of carbon and oxygen (see, e.g., Starrfield, Truran, Sparks, & Kutter (1972), and Starrfield, Sparks, & Truran (1974)) and just reflects the fact that we do not find much mixing by convective overshooting in the early phase of the TNR. The moderate increase of both maximum temperature and energy generation rate continues until most of the protons are used up after approximately 500 s.

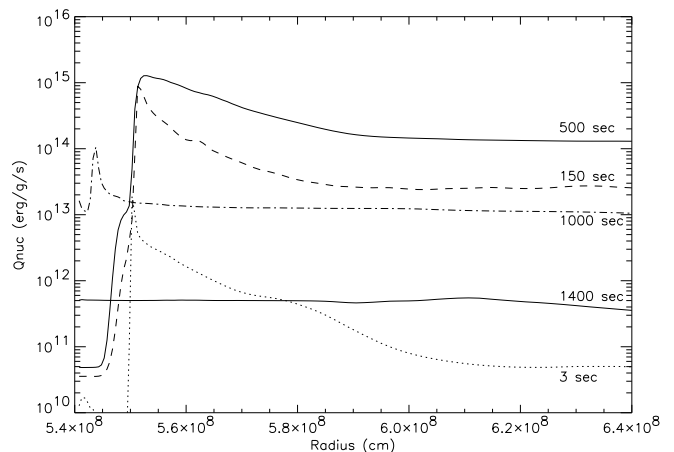


Fig. 2. Laterally averaged vertical profile of the energy production rate at several times of the low resolution calculation.

Fig. 1. Velocity field at different stages of the evolution for the low resolution run. The color coding is done according to the absolute value of the velocity at each point. T8 denotes the temperature of the hottest individual zone.

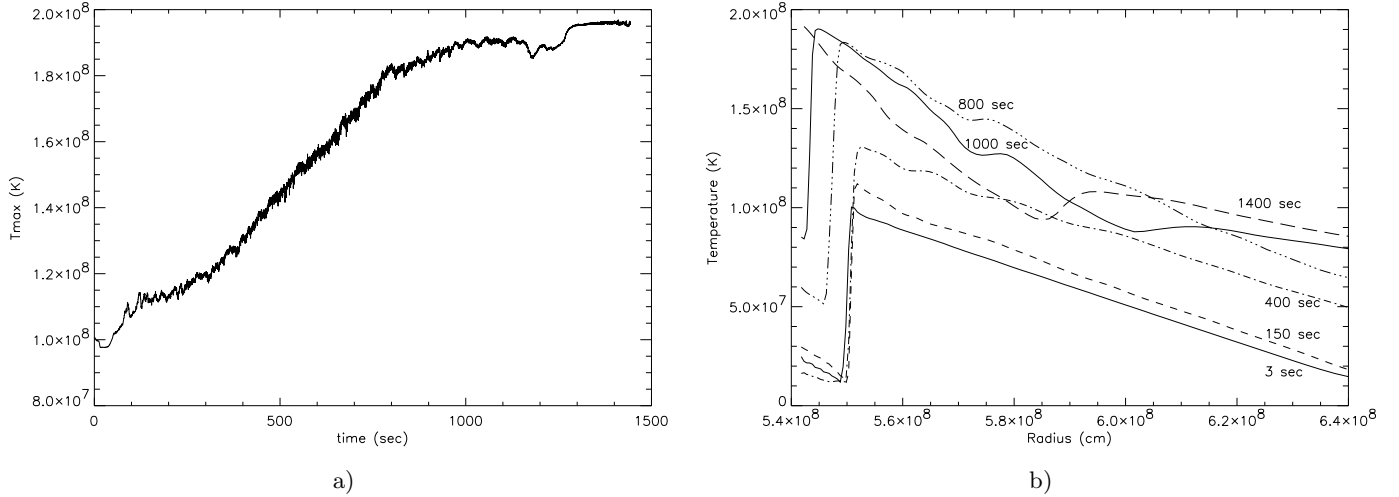


Fig. 3. Temperature evolution of the low resolution run. a) is the temperature of the hottest envelope shell and b) the laterally averaged vertical temperature profile at several times.

This behavior of our simulation, which is distinctly different from earlier 2-d work (i.e., Glasner, Livne & Truran (1997)) can be understood as follows. We find that during the first 100 to 150 seconds after ignition the flow field reaches a quasi-stationary state in which the whole envelope is convectively stirred up and the dominant eddy size is about 200 km only (Fig. 1e). These eddies appear to be very stable. They rarely merge to larger convective structures but rather behave like particles which scatter off after collisions, in contrast to what one expects to happen for homogeneous and isotropic 2-d turbulence. However, this finding is not new but has already been discussed in the turbulence literature much earlier (Fornberg (1977), Basdevant, Legras, Sadourny & Belánd (1981), and McWilliams (1984)). There it was suggested that the long time evolution of turbulent 2-d flow fields is dominated by small coherent vortices.

In order to clarify this point we will, in the following, give a short summary of the theoretical background of 2-d turbulence. In general, 2-d turbulence is the study of solutions of the incompressible Navier-Stokes equation which depend only on two cartesian coordinates, say x and y . Since we solve the Euler equation, we confine the discussion to the case when the viscosity ν is zero. According to Frisch (1995) the z component of the Euler equation is a simple advection diffusion equation without back reaction on the x - y plane. The vorticity has just a vertical component with respect to the x - y plane. Taking the curl of the Euler equation the vorticity equation follows which has, under the foregoing assumptions, just a z component which we denote by ζ . Introducing a stream function ψ by $V_x = \partial_y \psi$ and $V_y = -\partial_x \psi$ the vorticity equation of the

incompressible Euler equation reads :

$$\begin{aligned} \partial_t \zeta &= J(\psi, \zeta) + \eta \\ \Delta \psi &= -\zeta, \end{aligned} \quad (6)$$

where $J(\psi, \zeta) = \partial_x \psi \partial_y \zeta - \partial_x \zeta \partial_y \psi$ is the Jacobian Operator and η is the curl of the external driving force. This equation is vorticity conserving when viscosity (here of course $\nu = 0$) and external forces are ignored.

Because of the symmetry chosen we have $\nabla \times \nabla \phi = 0$ therefore $\eta = 0$. However, in our case we consider general compressible flows with energy sources and also numerical viscosity comes into play. As a consequence vorticity conservation is not exactly fulfilled. On the other hand, in situations where incompressibility is a good approximation and the energy source term is small vorticity is nearly conserved, and in fact we do find such situations in our simulations.

If one assumes that vorticity is exactly conserved the arguments in favour of stable coherent vortices proceed as follows: The solutions of

$$J(\psi, \Delta \psi) = 0 \quad (7)$$

are a subclass of solutions to eq. (6) for $\eta = 0$ in a suitable frame of reference where the vorticity ζ is not explicitly time dependent. This also includes axially symmetric circular vortices where the stream function ψ is just a function of the distance to the vortex center.

According to Frisch (1995) cascade arguments are not valid anymore because vorticity conservation guarantees the stability of those vortices, provided they are approximately axially symmetric. As was pointed out by Frisch (1995) such axi-symmetric structures behave like point vortices, as long as they are well separated from each

other, or like drops of 'laminar' fluid in an otherwise turbulent flow.

In our simulations we indeed do find these quasi-stable vortices, as long as the nuclear energy generation rate is moderate and the background flow on large scales is sub-sonic, such that incompressibility is a good approximation. They are responsible for the fact that we do not observe much overshooting and mixing during the first 150 s of the TNR. The maximum velocities of these eddies can get very close to sound speed (~ 1400 km/sec at 150 seconds) and may even exceed it later on. So a large part of the convective (and turbulent) kinetic energy is locked in structures which do not contribute significantly to the mixing. In contrast, typical velocities of the large scale background flow are a few 100 km/s at that time. The characteristic scale of a few 100 km is explained by numerical resolution effects at the lower end and the distortions of the axi-symmetry once their linear dimension approaches a pressure scale-height. So we expect that the typical scale will get smaller with increasing numerical resolution, and we indeed find this effect as will be shown in the next subsection.

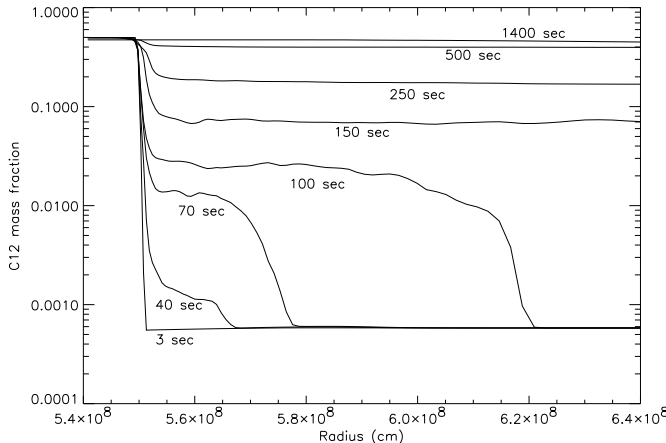


Fig. 4. Laterally averaged vertical profile of the ^{12}C mass fraction at several times of the low resolution calculation.

After about 150 seconds the most violently burning shells reach nearly the peak nuclear energy generation rate and stay approximately constant there (with very slow further increase) until the maximum is reached after about 500 seconds. During that phase the nuclear energy release still keeps rising gradually in the outer parts of the envelope (Fig. 2) due to radioactive decay heating caused by the enhancement of β^+ -unstable nuclei such as ^{15}O there, but the small-scale vortices gradually disappear. Our interpretation is that they are purely a consequence of inertial range turbulence (which explains why their typical scale is always smaller than the pressure scale-height) and they disappear once they are heavily distorted by nuclear energy generation. Consequently, we start to see considerable mixing of white dwarf core material into the envelope.

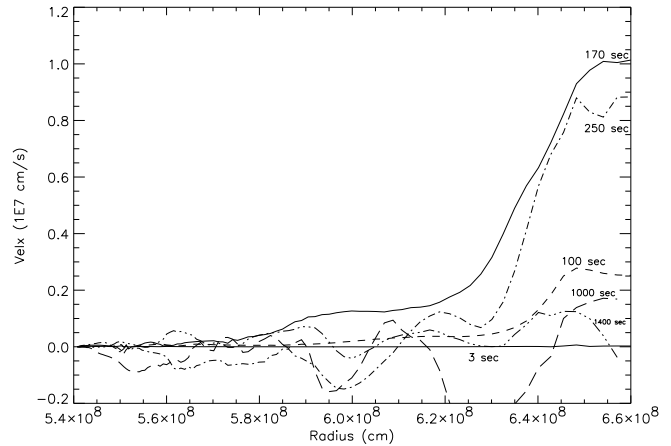


Fig. 5. Laterally averaged vertical profile of the vertical component of the velocity at several times of the low resolution calculation.

While in the earlier phase (until 150 s) the mixing of C and O into the envelope resulted in an overall ^{12}C mass fraction of only about 7% (Fig. 4), it now rises gradually to almost 40% at 500 s in that part of the envelope not lifted off the white dwarf.

The ^{12}C mass fraction and the envelope metallicity are measures for the dredge up of core material, since the CNO cycle does not lead to a higher number of CNO nuclei in the envelope but just distributes the shell metallicity among the different CNO nuclei. The spatial distributions of ^{12}C are shown in Figs. 10e and 10f at an early time (70 s) and later near the end of this phase (500 s). The distribution looks rather smooth (note that in going from panel e to f the color coding was changed), showing that the convective times are indeed short as compared to the nuclear burning time scale.

Also, envelope matter is expelled with velocities of up to 100 km/s at 170 s and beyond (Fig. 5), which leads to a remarkable decrease of the envelope's density (Fig. 6). It decreases until minimum values are reached after 300 s (Fig. 6). From then on mixing of core material into the envelope becomes very efficient, and C and O are mixed at a rate which leads to increasing the envelope density again. The flow field evolves from a state dominated by small eddies of scales of 200 km to one which looks very inhomogeneous and incoherent, dominated by large scale motions. Fig. 1f is representative for this phase, in which nuclear burning affects the flow patterns considerably.

During all of the phases discussed so far β^+ -unstable nuclei are produced in the burning region and are convectively spread over the entire envelope (Fig. 7, 10g,h). This is reflected in Fig. 2 by the nearly constant energy generation rates as a function of distance from the core. The horizontal tails seen in this figure are due to energy release by temperature independent β -decays, especially ^{15}O (Fig. 8) and ^{14}O . As long as the time scale for the

Time	^{14}O	^{15}O	^{17}F
800 sec	$1.0 \cdot 10^{14}$	$5.3 \cdot 10^{11}$	$2.8 \cdot 10^{11}$
1000 sec	$1.7 \cdot 10^{13}$	$1.6 \cdot 10^{11}$	$4.7 \cdot 10^{10}$
1200 sec	$2.7 \cdot 10^{12}$	$5.0 \cdot 10^{10}$	$6.5 \cdot 10^9$

Table 1 : Energy production rate contributions in erg/g/s of different β -unstable isotopes at different times calculated for the envelope shell at 6000 km. The dominant energy production in the outer parts of the envelope is due to the β -decay of ^{14}O .

production of ^{15}O is still shorter than its decay time we find an increasing mass fraction of ^{15}O , peak values being reached after roughly 800 s (Fig. 7). The fact that the temperature keeps rising and the energy generation rate drops more slowly than would be predicted from ^{15}O decay alone is due to the formation and decay of ^{14}O which sets in once the envelope has been enriched with core material (see Table 1).

At this time only a few protons are left in the envelope (Fig. 8) and the violent burning is close to being extinguishing. The dredge-up of core material yields a gradual removing of the outer parts of the white dwarf (Fig. 6) which becomes remarkable after about 1000 s. The energy production by radioactive decays gets low and the temperature increase levels off. Small scale vortices reappear, as is to be expected from the previous discussion.

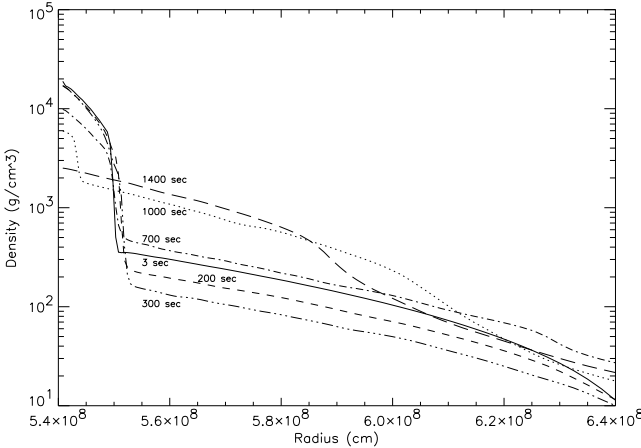


Fig. 6. Laterally averaged vertical profile of the density at several times of the low resolution calculation.

Protons which have been mixed into the cool core during previous stages (Fig. 8) and stored there and, due to low core temperatures, have not been fused by the CNO-cycle are now mixed into the envelope again. Here they are instantaneously absorbed via proton capture reactions almost exclusively in the hottest envelope shells resulting in a peak of the energy production there (Fig. 2). Although the effect of this extra burning on the over-all dynamics is not very big it may have interesting consequences for the nucleosynthesis yields expected from the outburst,

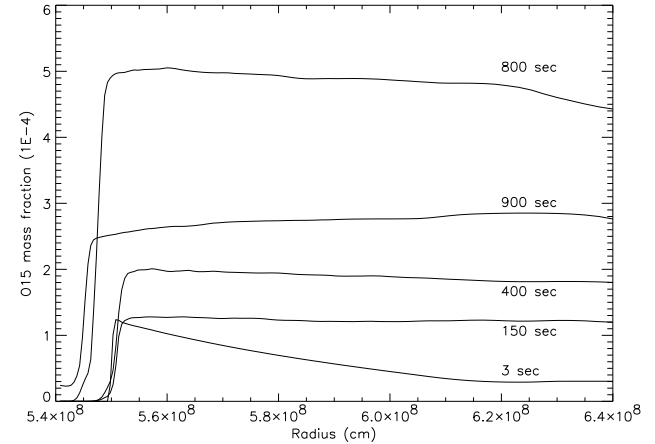


Fig. 7. Laterally averaged vertical profile of the ^{15}O mass fraction at several times of the low resolution calculation.

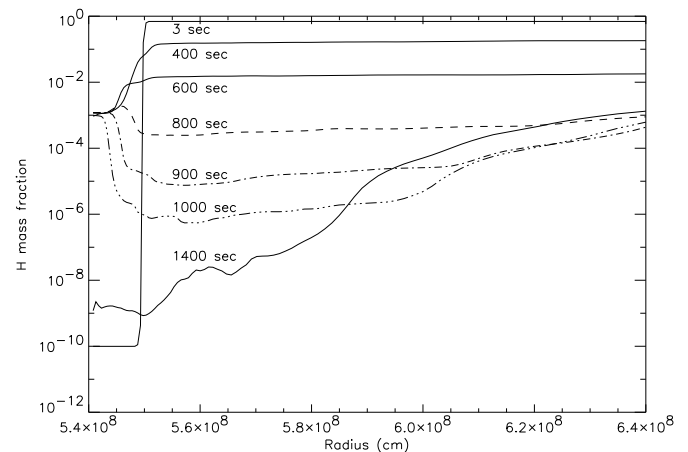


Fig. 8. Laterally averaged vertical profile of the proton mass fraction at several times of the low resolution calculation.

because a small fraction of it might be mixed convectively all the way to the surface.

The growing envelope mass and the slowly decreasing nuclear energy release leads to a decrease of outflow velocities, until the envelope almost stops expanding near the end of the computations (Fig. 5). Most of the outer core material covered by the computational grid has been mixed into the envelope by that time (Fig. 6). The convective velocities decrease steadily (Fig. 1h) and the envelope approaches a new hydrostatic equilibrium state. Most of the previously stirred up heavy element enriched matter is settling onto the surface of the white dwarf at the end of the simulations (Fig. 6). The formation of a new core-envelope boundary is evident from the smooth density transition seen in Fig. 6 at 1000 and 1400 seconds, respectively, which is also visible in other observables like temperature (Fig. 3b) or hydrogen mass fraction (Fig. 8).

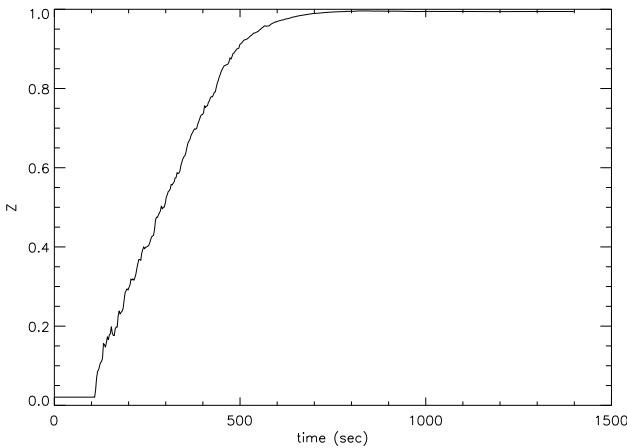


Fig. 9. Evolution of metallicity for the last five shells of the simulated envelope domain for the low resolution run.

Finally, in Fig. 9 we show how the metallicity of the ejected envelope material evolves with time. In order to do so we estimate the metallicity in the upper five calculated shells of the envelope and assume that they will be ejected. The values we obtain in this way are $Z \simeq 0.2\%$ for the maximum outflow velocities around 170 s, increasing up to about $Z = 0.9\%$ after 500 s when the outflow velocities are still remarkable.

3.2. The high resolution simulation

Increasing the resolution of the grid by a factor of five in each spatial direction means that computational costs increase by roughly a factor of 125 (including the effect of a five times smaller CFL-time step). So it is obvious that we could not compute a model with this resolution to the end of the TNR as was done for the previous run. However, since here we are more interested in testing the numerical accuracy of our attempt to simulate directly turbulent combustion in the accreted envelope of a white dwarf rather than presenting very realistic models for a nova outburst which can be compared with observations (what in fact could be done and will be done in a forthcoming paper since all the relevant physics is included in the code), we decided to go for the high resolution and to follow the highly resolved model as long as necessary and possible. In practice this meant that we stopped the computations after a physical time of about 180 s, for reasons which will be discussed later.

Figure 11 gives the velocity field at different times for the case of high resolution and should be compared with Fig. 1 of the low resolution run. We disturbed as before one zone with a temperature amplitude of 1 %. Because now the mass inside a single zone is much smaller, the energy perturbation is about 20 times smaller as compared to the low resolution case. Naively one expects a somewhat slower evolution in the beginning, and that is exactly

what happens. We begin with showing a first snapshot at 13 s (Fig. 9a) since then the distortion is comparable (in energy) to the low resolution case after 3 s.

From then on the evolution of the TNR has many similarities but also distinct differences to the previous one. It is evident from Fig. 11 that the high resolution run also yields small coherent vortices, but now on typical length scales of 40 to 50 km which are smaller compared to the low resolution run by almost exactly the same factor by which the resolution was increased, indicating that these structures are still not fully resolved. Therefore, if it should turn out that the over-all properties of the model are affected in a similar manner this would mean that there is no chance to tackle the nova problem by means of direct numerical simulations. Independent of this practical question, it is interesting to see that again the small eddies seem to carry a considerable amount of the turbulent kinetic energy. This finding gives us some hope that 2-d simulations can capture essential features and that going to 3-d models might not be necessary, but, of course, this conjecture has to be tested.

The ignition phase is characterized by a flow field dominated by these small scale vortices. Their typical velocities rise more rapidly. For instance the maximum velocities after 70 seconds for the low resolution run are comparable to those of the high resolution run after 30 seconds. A likely interpretation is that now the characteristic size of these eddies is considerably smaller than the pressure scale height. Therefore they are less effected by potential energy differences. Note that the fastest structures dominate the color coding of Fig. 11 since we used a linear color scale.

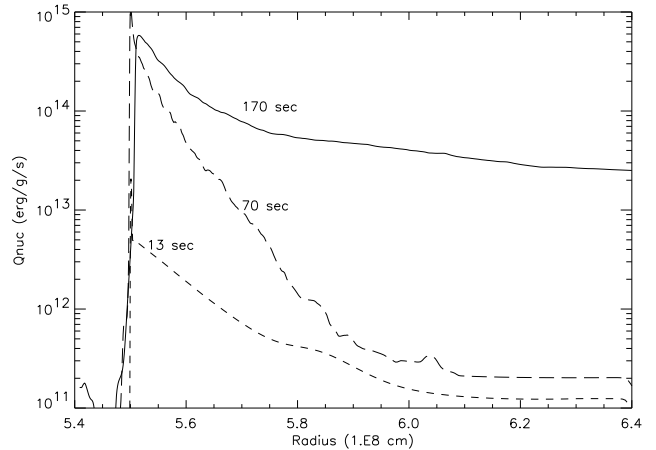


Fig. 12. Laterally averaged vertical profile of the energy production rate at several times of the high resolution calculation.

According to Fig. 11a,b,c the lateral spread of the burning by small scale turbulence along the white dwarf surface proceeds at a velocity of approximately 10 km/s

Fig. 10. Evolution of some of the quantities shortly after ignition (70 seconds) and at peak energy generation rate (500 seconds).

Fig. 11. Velocity field at different stages of the evolution for the high resolution run. The color coding is done according to the absolute value of the velocity at each point. T8 denotes the temperature of the hottest individual zone.

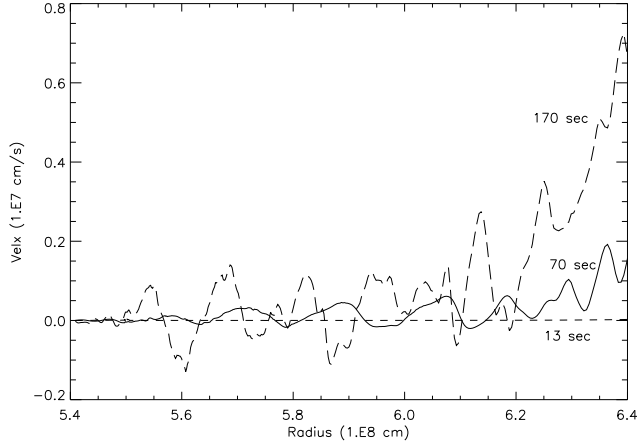


Fig. 13. Laterally averaged vertical profile of the vertical component of the velocity at several times of the high resolution calculation.

during the ignition phase, very similar to what we have found in the low resolution case, and in accord with the estimates of Fryxell & Woosley (1982). From then on again sound waves ignite the burning in other parts of the bottom shell of the envelope and they can also be seen propagating vertically in Fig. 11d. After about 40 s the entire bottom layer is burning. So the time required to propagate the front is equal to what we have found for lower resolution. This result is in agreement with the sound wave interpretation because the sound velocity is independent of the resolution. It also demonstrates that at least during the ignition phase *lateral* energy transport is not dominated by the fast moving small structures. However, the *vertical* extend of the convective region is affected as can be seen by comparing panel d of Fig. 1 with panel e of Fig. 11 but the convective energy is mainly locked in small scale motions.

As a result, we find that the temperatures in the hottest zones increase a bit faster than previously (Fig. 12a), but the over all effect is rather small as one can see by comparing the laterally averaged temperatures given in Fig. 3b and Fig. 12b. This is a clear indication that larger scales are mainly responsible for the energy transport, and they are well resolved in both cases. The small delay of the temperature increase in the low resolution run just reflects the fact that due to the lower velocities in the small eddies more energy is available for the large scale motions and, therefore, convective energy transport is a bit more effi-

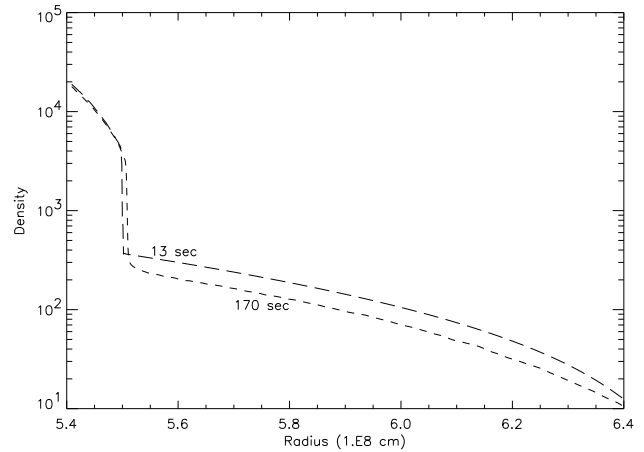


Fig. 14. Laterally averaged vertical profile of the density at several times of the high resolution calculation.

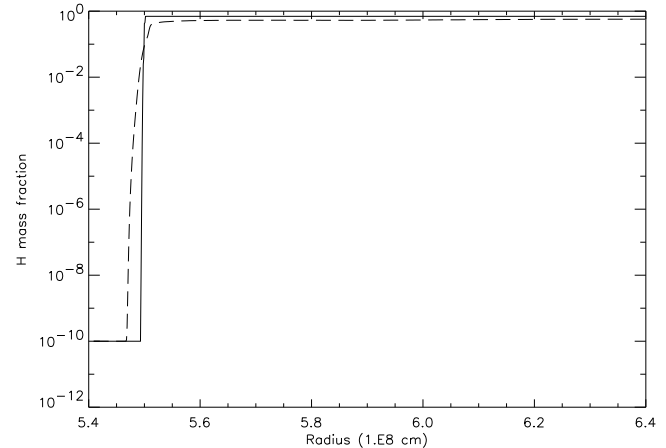


Fig. 15. Laterally averaged vertical profile of the proton mass fraction at several times of the high resolution calculation. Solid line : 13 seconds, dashed line : 170 seconds.

cient. It is also obvious from comparing for example Fig. 2 and Fig. 12 or Fig. 4 and Fig. 17 that there are only minor differences between the two calculations for key quantities such as the energy generation rate or the ^{12}C mass fractions once the envelope has become fully convective after about 150 s. This, in fact, was the main reason why we stopped the highly resolved run after about 180 s.

However, there is still a bit of uncertainty in this conclusion. It appears that in the high resolution case the

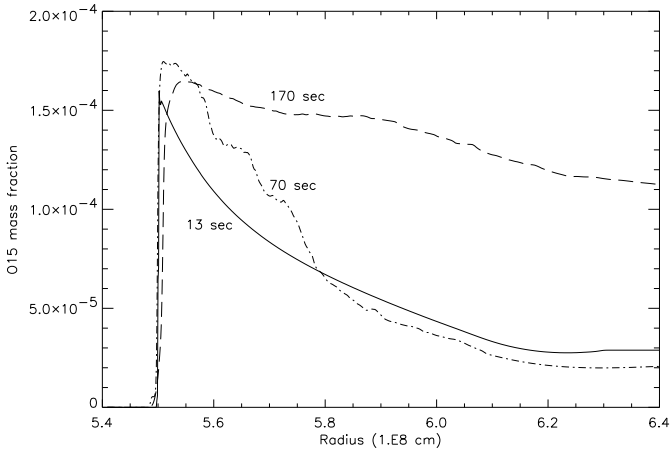


Fig. 16. Laterally averaged vertical profile of the ^{15}O mass fraction at several times of the high resolution calculation.

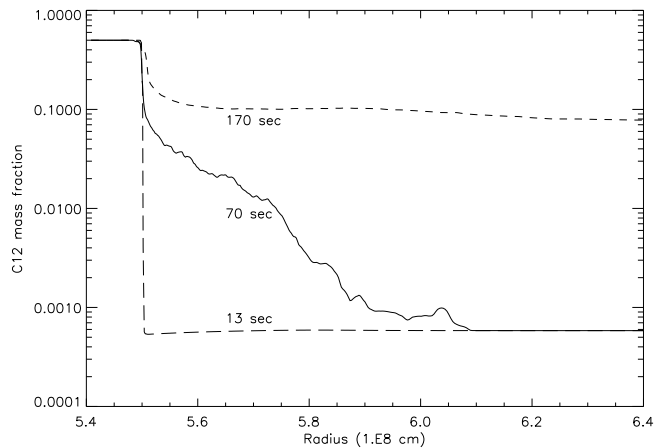


Fig. 17. Laterally averaged vertical profile of the ^{12}C mass fraction at several times of the high resolution calculation.

energy generation rate as well as the maximum temperature reached in any of the shells seems to decrease or at least level off after about 150s. We believe that this is a temporary effect only. As we have shown earlier, once the energy generation rate has reached values around 10^{15} erg/g/s the small vortices begin to be destroyed by the more violent large scale motions. It is very likely that the same will happen also in the high resolution calculations, maybe with some delay, due to the higher velocities (and therefore increased stability) in the smaller eddies.

Fig. 14 shows the laterally averaged vertical distribution of the vertical velocity component. Not surprisingly, the high resolution run shows much more structure and rapid oscillation, especially still at 170 seconds, whereas in the low resolution case the envelope is expanding more uniformly at the time of peak outflow velocities (Fig. 5), and they compare more with values reached already after

150 s in the latter. But again, we consider this to be a minor uncertainty, consistent with the general trend that for the better resolved calculations the early phase of the TNR proceeds a bit faster, whereas later, when larger eddies take over, the evolution is somewhat slower in this case.

The density profiles (Fig. 15) show the decrease of the envelope density. Just as before, consumption of protons also proceeds slowly (Fig. 16). For completeness, we give the ^{15}O mass fraction and metallicity of the ejected shells in Figs. 17 and 9, respectively. Of course, it would have been nice to give all these data also at later times, but because of the enormous computer time required for this run we stopped it.

4. Discussion and conclusions

We have presented first results of numerical simulations of the TNR in the hydrogen-rich envelope of an accreting white dwarf. These simulations were performed by means of a modified version of a standard PPM-type hydro code which is able to treat reactive hydrodynamics in one, two or three spatial dimensions. The models outlined in the previous sections were obtained in planar geometry, the surface layers of the white dwarf and its envelope being mapped onto a 2-d grid in Cartesian coordinates. The main intention of the simulations was to investigate the question as to whether convective overshooting can or will lead to self-enrichment of the envelope with C and O from the underlying white dwarf's surface.

The same question was recently addressed in a very similar simulation by Glasner, Livne & Truran (1997) who found in fact a positive result. According to their study, considerable dredge-up of white dwarf matter occurs early in the TNR, already after about 100 s, leading to a violent runaway between 150 and 200 s after the computations had been started in 2-d, with a temperature of 10^8K at the bottom of the envelope.

Our results agree in certain respects with those of Glasner, Livne & Truran (1997), and disagree in others. We agree with them on the general outcome, namely that even with an initially solar composition of the accreted matter most of the envelope is ejected during the outburst. We also agree that the ejected material will be enriched with matter mixed in from the white dwarf. On the other hand, the differences are remarkable, given the facts that we started our calculations from exactly the same initial conditions and that, in one case, even the numerical resolution was nearly equal to theirs.

In general terms, the outburst is much less violent in our calculations as compared to theirs. This shows up in the longer timescale for the TNR, the lower ejection velocities, the considerably lower temperature near peak energy production, etc.

The cause of the deviations can be traced back to large differences in the convective flow patterns we obtain. In

their simulations a few large eddies dominate the flow already during early phases of the TNR, whereas in our calculations small eddies carry a large amount of the convective kinetic energy until the burning proceeds at maximum rate. In Fig. 18 we provide energy spectra for the low resolution run, to support this argument. They are not as steep as expected for instance for unforced decaying incompressible turbulence as demonstrated in McWilliams (1984).

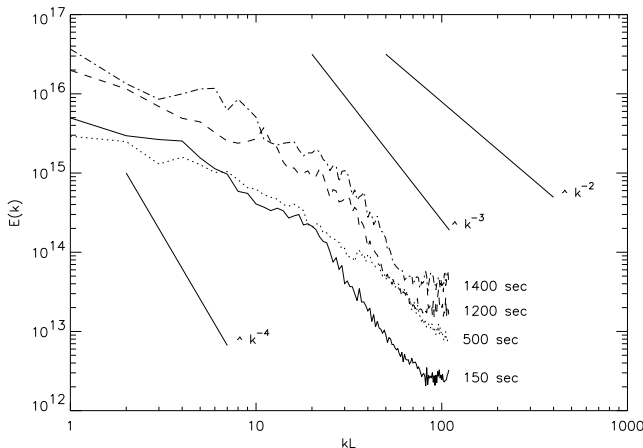


Fig. 18. Energy spectra of the kinetic energy at different times of the low resolution run. k is the wavenumber and L is the lateral gridlength. The energy is plotted in arbitrary units.

Most of these eddies move very little in vertical direction and, therefore, do not penetrate into the white dwarf. This is the reason why we observe very little mixing until the envelope lift-off sets in and dredge-up happens in the steep density (and pressure) gradient near the white dwarf's surface. However, this late mixing has little effect on the dynamical evolution of the envelope because at that stage most of the hydrogen has already been burnt.

If true, this finding will, nevertheless, affect the nucleosynthesis predictions obtained from the model, but we are not 100% sure. The reason is that the surface layers of the white dwarf are not well resolved in our "low" resolution run and, due to the Eulerian nature of the code numerical diffusion may in part be responsible for some of the late mixing. In principle this could be checked by extending the "high" resolution run to about 800 s, but this would cost a lot of computer resources, and we thought it might be more important to save those for 3-d simulations which are under way.

The question then remains as to why the flow patterns are so different in the two independent sets of calculations. Our interpretation is that they are mainly caused by the different boundary conditions and symmetries imposed. We think it is dangerous to impose polar symmetry and reflecting boundary conditions in simulations

which aim at investigating geometrical properties of free subsonic convection. In fact, we found in our simulations that the fast and small vortices moved mainly horizontally all across the computational grid, leaving the grid on one side and coming back from the other. Such motions would be prohibited if reflecting boundaries were imposed, and it is likely that such boundary conditions will suppress these modes. Moreover, as can be seen in Fig. 1 and 2 of Glasner, Livne & Truran (1997) in their computations most of the action appears to be either at the polar axis or near the horizontal boundaries which indicates unphysical symmetries.

In conclusion, we have demonstrated that direct numerical simulations of thermonuclear combustion in the accreted hydrogen-rich envelopes of white dwarfs are feasible. We have shown that even in 2-d (and in contrast to common expectations) small scale structures carry a large amount of the convective kinetic energy. The smallest of those eddies were not resolved in our models but their actual size seems to be of minor importance for the general behavior of the TNR. Just the fact that they exist makes a big difference, as the comparison with the work of Glasner, Livne & Truran (1997) showed. They were interpreted as stable solutions of the (time independent) Euler equations which form from small fluctuations in 2-d convective flows. The fact that they disappeared once the energy generation (source terms) began to dominate over the advection strongly supports this interpretation.

It will be interesting to see which of these conclusions remain valid in 3-d simulations. The small scale vortices might not be as important any more because their stability rests largely on axi-symmetry which is broken in 3-d. On the other hand side, their main effect was to hinder the formation of dominant large scale eddies which otherwise would show up more clearly in 2-d. So there is hope that 2-d simulations do capture the main features of the TNR, but this has to be seen.

Acknowledgements. The authors are grateful for many enlightening discussions with Stanford E. Woosley, Jens C. Niemeyer and Ulrich Kolb. They thank Ami Glasner and Eli Livne for supplying the initial model, Ewald Müller for an earlier version of the PROMETHEUS code, and Rudi Fischer and Jakob Pichlmeier for their help in preparing a parallel version of the code. They also thank the staff members of the Rechenzentrum Garching for their support during the computations. This work was supported in part by NSF at the Institute for Theoretical Physics at the University of California, Santa Barbara under Grant No. PHY94-07194 and by NASA under Grant NAG 5-3076 at the University of Chicago. The computations were performed at the Rechenzentrum Garching on a Cray T3E.

References

Basdevant, C., Legras, B., Sadourny, R., and Belánd, M., 1981, *J. Atmos. Sci.*, 38, 2305

Colella, P., and Woodward, P.R., 1984, *J. Comp. Physics*, 54, 174

Fornberg, B., 1977, *J. Comp. Physics*, 25, 1

Frisch, U., *Turbulence*, Cambridge University Press 1995

Fryxell, B.A., and Woosley, S.E., 1982, *ApJ*, 261, 332

Fryxell, B.A., Müller, E., and Arnett, W.D., 1989, Max-Planck-Institut für Astrophysik Report 449, Garching, Germany

Glasner, S.A., and Livne, E., 1995, *ApJ*, 445, L149

Glasner, S.A., Livne E., and Truran, J.W., 1995, in IAU Colloq. 158, *Cataclysmic Variables and Related Objects*, ed. E. Evans & J.H. Wood (Kluwer: Academic), in press

Glasner, S.A., and Truran J.W., 1996, in preparation

Glasner, S.A., and Livne E., and Truran, J.W., 1997, *ApJ*, 475, 754

Livne, E., 1993, *ApJ*, 412, 634

Mac Donald, J., 1980, *MNRAS*, 191, 933

McWilliams, J.C., 1984, *J. Fluid Mech.*, 146, 21

Müller, E., 1986, *A&A*, 162, 103

Müller, E., 1994, in *Supernovae* (Proc. Les Houches Summer School 1991), ed. S.A. Bludman, R. Mochkovitch, and J. Zinn-Justin (Amsterdam:Elsevier), p. 395

Müller, E., 1997, in *Gravitational Radiation* (Proc. Les Houches Summer School 1995), ed. S. Bonazzola and J.-A. Marck (Cambridge:Cambridge Univ. Press), in press

Niemeyer, J.C., and Hillebrandt, W., 1995, *ApJ*, 452, 779

Prialnik, D., Shara, M.M., and Shaviv, G., 1978, *A&A*, 62, 339

Shankar, A., and Arnett, W.D., Fryxell, B. A., 1992, *ApJ*, 394, L13

Shankar, A., and Arnett, W.D., 1994, *ApJ*, 433, 216

Shara, M.M., 1981, *ApJ*, 243, 926, 1982, *ApJ*, 261, 649

Spiegel, E.A., 1963, *ApJ*, 138, 216

Starrfield, S., 1989, in *The Classical Novae*, ed. M. Bode and A. Evans, (Wiley: NY), 39

Starrfield, S., 1993, in *The Realm of Interacting Binary Stars*, ed. J. Sahade, G.E. McCluskey, and Y. Kondo (Dordrecht: Kluwer), 209

Starrfield, S., 1995, in *Physical Processes in Astrophysics*, ed. I. Roxburgh, and J.L. Masnou, (Springer: Heidelberg), 99

Starrfield, S., Sparks, W.M., and Truran, J.W., 1974, *ApJ Suppl.*, 28, 247, 1985, *ApJ*, 291, 136

Starrfield, S., Truran, J.W., Sparks, W.M., and Kutter, G.S., 1972, *ApJ*, 176, 169

Thielemann, F.-K., 1996, private communication

Truran, J.W., 1982, in *Essays in Nuclear Physics*, ed. C.A. Barnes, D.D. Clayton and D.N. Schramm (Cambridge: Cambridge U. Press), 467

Truran, J.W., 1990, in *The Physics of Classical Novae*, ed. A. Cassatella and R. Viotti, (Heidelberg: Springer), 373

Wallace, R.K., and Woosley, S.E., 1981, *ApJS*, 45, 389

Woosley, S.E., 1986, in *Nucleosynthesis and Chemical Evolution*, ed. B. Hauck, A. Maeder, and G. Magnet (Sauverny:Geneva Observatory)

This figure "figure1.gif" is available in "gif" format from:

<http://arxiv.org/ps/astro-ph/9801054v2>

This figure "figure10.gif" is available in "gif" format from:

<http://arxiv.org/ps/astro-ph/9801054v2>

This figure "figure11.gif" is available in "gif" format from:

<http://arxiv.org/ps/astro-ph/9801054v2>